

An improved measurement of muon antineutrino disappearance in MINOS

P. Adamson,⁷ D. S. Ayres,¹ C. Backhouse,¹⁸ G. Barr,¹⁸ M. Bishai,³ A. Blake,⁵ G. J. Bock,⁷ D. J. Boehnlein,⁷ D. Bogert,⁷ S. V. Cao,²⁶ S. Childress,⁷ J. A. B. Coelho,⁶ L. Corwin,¹² D. Cronin-Hennessy,¹⁵ I. Z. Danko,¹⁹ J. K. de Jong,¹⁸ N. E. Devenish,²⁴ M. V. Diwan,³ C. O. Escobar,⁶ J. J. Evans,¹⁴ E. Falk,²⁴ G. J. Feldman,⁹ M. V. Frohne,¹⁰ H. R. Gallagher,²⁷ R. A. Gomes,⁸ M. C. Goodman,¹ P. Gouffon,²¹ N. Graf,¹¹ R. Gran,¹⁶ K. Grzelak,²⁸ A. Habig,¹⁶ J. Hartnell,²⁴ R. Hatcher,⁷ A. Himmel,⁴ A. Holin,¹⁴ X. Huang,¹ J. Hyslop,⁷ G. M. Irwin,²³ Z. Ivan,¹⁹ D. E. Jaffe,³ C. James,⁷ D. Jensen,⁷ T. Kafka,²⁷ S. M. S. Kasahara,¹⁵ G. Koizumi,⁷ S. Kopp,²⁶ M. Kordosky,²⁹ A. Kreymer,⁷ K. Lang,²⁶ J. Ling,^{3,22} P. J. Litchfield,^{15,20} L. Loiacono,²⁶ P. Lucas,⁷ W. A. Mann,²⁷ M. L. Marshak,¹⁵ M. Mathis,²⁹ N. Mayer,¹² R. Mehdiyev,²⁶ J. R. Meier,¹⁵ M. D. Messier,¹² D. G. Michael,^{4,*} W. H. Miller,¹⁵ S. R. Mishra,²² J. Mitchell,⁵ C. D. Moore,⁷ L. Mualem,⁴ S. Mufson,¹² J. Musser,¹² D. Naples,¹⁹ J. K. Nelson,²⁹ H. B. Newman,⁴ R. J. Nichol,¹⁴ J. A. Nowak,¹⁵ W. P. Oliver,²⁷ M. Orchanian,⁴ R. B. Pahlka,⁷ J. Paley,^{1,12} R. B. Patterson,⁴ G. Pawloski,^{15,23} S. Phan-Budd,¹ R. K. Plunkett,⁷ X. Qiu,²³ A. Radovic,¹⁴ J. Ratchford,²⁶ B. Rebel,⁷ C. Rosenfeld,²² H. A. Rubin,¹¹ M. C. Sanchez,^{13,1,9} J. Schneps,²⁷ A. Schreckenberger,¹⁵ P. Schreiner,¹ R. Sharma,⁷ A. Sousa,⁹ M. Strait,¹⁵ N. Tagg,¹⁷ R. L. Talaga,¹ J. Thomas,¹⁴ M. A. Thomson,⁵ G. Tinti,¹⁸ R. Toner,⁵ D. Torretta,⁷ G. Tzanakos,² J. Urheim,¹² P. Vahle,²⁹ B. Viren,³ J. J. Walding,²⁹ A. Weber,^{18,20} R. C. Webb,²⁵ C. White,¹¹ L. Whitehead,³ S. G. Wojcicki,²³ and R. Zwaska⁷

(The MINOS Collaboration)

¹Argonne National Laboratory, Argonne, Illinois 60439, USA²Department of Physics, University of Athens, GR-15771 Athens, Greece³Brookhaven National Laboratory, Upton, New York 11973, USA⁴Lauritsen Laboratory, California Institute of Technology, Pasadena, California 91125, USA⁵Cavendish Laboratory, University of Cambridge, Madingley Road, Cambridge CB3 0HE, United Kingdom⁶Universidade Estadual de Campinas, IFGW-UNICAMP, CP 6165, 13083-970, Campinas, SP, Brazil⁷Fermi National Accelerator Laboratory, Batavia, Illinois 60510, USA⁸Instituto de Física, Universidade Federal de Goiás, CP 131, 74001-970, Goiânia, GO, Brazil⁹Department of Physics, Harvard University, Cambridge, Massachusetts 02138, USA¹⁰Holy Cross College, Notre Dame, Indiana 46556, USA¹¹Department of Physics, Illinois Institute of Technology, Chicago, Illinois 60616, USA¹²Indiana University, Bloomington, Indiana 47405, USA¹³Department of Physics and Astronomy, Iowa State University, Ames, Iowa 50011 USA¹⁴Department of Physics and Astronomy, University College London, Gower Street, London WC1E 6BT, United Kingdom¹⁵University of Minnesota, Minneapolis, Minnesota 55455, USA¹⁶Department of Physics, University of Minnesota – Duluth, Duluth, Minnesota 55812, USA¹⁷Otterbein College, Westerville, Ohio 43081, USA¹⁸Subdepartment of Particle Physics, University of Oxford, Oxford OX1 3RH, United Kingdom¹⁹Department of Physics and Astronomy, University of Pittsburgh, Pittsburgh, Pennsylvania 15260, USA²⁰Rutherford Appleton Laboratory, Science and Technologies Facilities Council, OX11 0QX, United Kingdom²¹Instituto de Física, Universidade de São Paulo, CP 66318, 05315-970, São Paulo, SP, Brazil²²Department of Physics and Astronomy, University of South Carolina, Columbia, South Carolina 29208, USA²³Department of Physics, Stanford University, Stanford, California 94305, USA²⁴Department of Physics and Astronomy, University of Sussex, Falmer, Brighton BN1 9QH, United Kingdom²⁵Physics Department, Texas A&M University, College Station, Texas 77843, USA²⁶Department of Physics, University of Texas at Austin, 1 University Station C1600, Austin, Texas 78712, USA²⁷Physics Department, Tufts University, Medford, Massachusetts 02155, USA²⁸Department of Physics, University of Warsaw, Hoża 69, PL-00-681 Warsaw, Poland²⁹Department of Physics, College of William & Mary, Williamsburg, Virginia 23187, USA

(Dated: Jan 19, 2012)

We report an improved measurement of $\bar{\nu}_\mu$ disappearance over a distance of 735 km using the MINOS detectors and the Fermilab Main Injector neutrino beam in a $\bar{\nu}_\mu$ -enhanced configuration. From a total exposure of 2.95×10^{20} protons on target, of which 42% have not been previously analyzed, we make the most precise measurement of $\Delta\bar{m}^2 = [2.62_{-0.28}^{+0.31}(\text{stat.}) \pm 0.09(\text{syst.})] \times 10^{-3} \text{eV}^2$ and constrain the $\bar{\nu}_\mu$ mixing angle $\sin^2(2\bar{\theta}) > 0.75$ (90%CL). These values are in agreement with Δm^2 and $\sin^2(2\theta)$ measured for ν_μ , removing the tension reported in [1].

PACS numbers: 14.60.Pq, 14.60.Lm, 29.27.-a

Observations of neutrinos and antineutrinos created in the Sun, the Earth's atmosphere, reactors and acceler-

ators provide strong evidence [2–10] that neutrinos undergo transitions between their flavor eigenstates (ν_e , ν_μ , ν_τ) as they propagate. These transitions can occur due to quantum mechanical mixing between the neutrino flavor and mass (ν_1 , ν_2 , ν_3) eigenstates. The mixing may be parametrized with a unitary matrix U_{PMNS} [11] which is typically expressed in terms of three mixing angles θ_{12} , θ_{23} , θ_{13} and a charge-parity (CP) violating phase δ . This interpretation, referred to as “neutrino oscillations,” requires that neutrinos have mass and motivates extensions to the Standard Model (SM) of particle physics. Extensions which explain the origin of neutrino masses, for example the addition of right handed sterile neutrinos ν_R [12], may also explain the baryon asymmetry [13] of the universe.

The CPT symmetry of the SM requires that ν_μ and $\bar{\nu}_\mu$ have the same masses and mixing parameters. In vacuum, the probability $P(\nu_\mu \rightarrow \nu_\mu)$ that a ν_μ is detected after a distance L as a ν_μ (rather than a ν_e or ν_τ) must be equal to the corresponding probability $P(\bar{\nu}_\mu \rightarrow \bar{\nu}_\mu)$ for antineutrinos. For a ν_μ with energy E the probability may be written as

$$P(\nu_\mu \rightarrow \nu_\mu) = 1 - \sin^2(2\theta) \sin^2 \left(\frac{1.267 \Delta m^2 [\text{eV}^2] L [\text{km}]}{E [\text{GeV}]} \right) \quad (1)$$

where Δm^2 and $\sin^2(2\theta)$ are effective parameters that are functions of the angles parameterizing U_{PMNS} and the differences in the squared masses $\Delta m_{ij}^2 = m_i^2 - m_j^2$ of the ν_1 , ν_2 and ν_3 states. Experiments have demonstrated $|\Delta m_{31}^2| \gg |\Delta m_{21}^2|$ [14]. In the limiting case that $\theta_{13} \approx 0$ we have $\theta \approx \theta_{23}$ and $|\Delta m^2| \approx \sin^2(2\theta_{12}) |\Delta m_{31}^2| + \cos^2(2\theta_{12}) |\Delta m_{32}^2|$ [15, 16]. Muon antineutrino oscillations are described by an equation which has the same form as Eq. 1 with parameters $\Delta \bar{m}^2$ and $\sin^2(2\bar{\theta})$. The extended SM predicts $\Delta \bar{m}^2 = \Delta m^2$ and $\sin^2(2\bar{\theta}) = \sin^2(2\theta)$ for vacuum oscillations [17, 18]. Observation of $P(\nu_\mu \rightarrow \nu_\mu) \neq P(\bar{\nu}_\mu \rightarrow \bar{\nu}_\mu)$ would therefore be evidence for physics beyond the SM, such as neutrino interactions in the earth’s crust that do not conserve lepton flavor.

In this Letter we describe a measurement of $P(\bar{\nu}_\mu \rightarrow \bar{\nu}_\mu)$ conducted over a baseline $L = 735$ km using a $\bar{\nu}_\mu$ -enhanced beam with a peak energy of 3 GeV. The beam was produced by directing 120 GeV/c protons from the Fermilab Main Injector onto a graphite target to produce π/K mesons that decay to produce neutrinos. Two magnetic horns focus the mesons, allowing us to control the energy spectrum and $\nu/\bar{\nu}$ content of the beam.

The neutrino beam is pointed towards two detectors, referred to as Near and Far. The 980 ton Near Detector (ND) measures the ν_μ and $\bar{\nu}_\mu$ content of the beam as a function of energy at a distance of 1.04 km from the π/K production target. The 5.4 kton Far Detector (FD) is located in the Soudan Underground Laboratory, 734 km from the ND, and remeasures the beam composition. The neutrino detectors are steel-scintillator,

tracking-sampling calorimeters optimized to identify and measure the energy of muon neutrinos and antineutrinos and reject backgrounds from neutral current and ν_e interactions [19]. The detectors are magnetized with an average field of 1.3 T to distinguish ν_μ from $\bar{\nu}_\mu$ based on the charge of the μ produced in weak interactions.

We previously reported ν_μ oscillations with an energy dependence consistent with Eq. 1 and $\Delta m^2 = 2.32_{-0.08}^{+0.12} (\text{stat.} + \text{syst.}) \times 10^{-3} \text{eV}^2$, $\sin^2(2\theta) > 0.90$ (90% CL) [4]. The measurements utilized 7.25×10^{20} protons on target (POT) of data collected between 2005-2009 with a ν_μ -enhanced beam [20]. Measurements made by Super-Kamiokande [5] and T2K [21] are in good agreement with our values.

In 2009-2010 we collected 1.71×10^{20} POT in a $\bar{\nu}_\mu$ -enhanced beam [20] created by reversing the polarity of the horns. The magnetic fields in the FD and ND were also reversed to focus the μ^+ created in $\bar{\nu}_\mu$ interactions. These antineutrino data also exhibited oscillations in agreement with Eq. 1, but with parameters $\Delta \bar{m}^2 = [3.36_{-0.40}^{+0.46} (\text{stat.}) \pm 0.06 (\text{syst.})] \times 10^{-3} \text{eV}^2$ and $\sin^2(2\bar{\theta}) = 0.86 \pm 0.11 (\text{stat.}) \pm 0.01 (\text{syst.})$ [1]. We found no systematic effects which could explain the difference between the ν_μ and $\bar{\nu}_\mu$ parameters. Assuming identical true values for $(\Delta \bar{m}^2, \sin^2(2\bar{\theta}))$ and $(\Delta m^2, \sin^2(2\theta))$, we calculated that such a difference would occur by random chance about 2% of the time. To clarify the situation we collected an additional 1.24×10^{20} POT with the $\bar{\nu}_\mu$ -enhanced beam during 2010-2011. We have also updated the analysis to improve the sensitivity to $(\Delta \bar{m}^2, \sin^2(2\bar{\theta}))$, reduce uncertainties due to Monte Carlo (MC) modeling in the ND, and increase the similarity to the ν_μ oscillation analysis.

We isolate a sample of ν_μ and $\bar{\nu}_\mu$ charged-current (CC) $\nu_\mu N \rightarrow \mu X$ events by searching for interaction vertices inside our detectors with a muon track and possible hadronic activity from the recoil system X . We reject hadron tracks reconstructed in neutral-current (NC) events by combining four topological variables describing track properties into a single discriminant variable, μID , using a k -nearest-neighbor (kNN) technique [22]. The kNN algorithm calculates the distance in the four-variable space between each measured event and an ensemble of simulated events; the output is the fraction of signal in the $k = 80$ closest MC events. This discriminant was used in our previous analyses [1, 4] and, as shown in Fig. 1(a), is well modeled by our MC. We maximize the statistical sensitivity to $\Delta \bar{m}^2$ by requiring $\mu\text{ID} > 0.3$, which results in a MC estimated efficiency/purity of 90.7%/99.0% at the ND and 91.6%/99.0% at the FD. We then discriminate ν_μ from $\bar{\nu}_\mu$ on an event-by-event basis by analyzing the track curvature in the detector’s magnetic field. Figure 1(b) shows the track charge/momentum (q/p) divided by its uncertainty ($\sigma(q/p)$), as determined by our track reconstruction algorithm. We select $\bar{\nu}_\mu$ and reject ν_μ by requir-

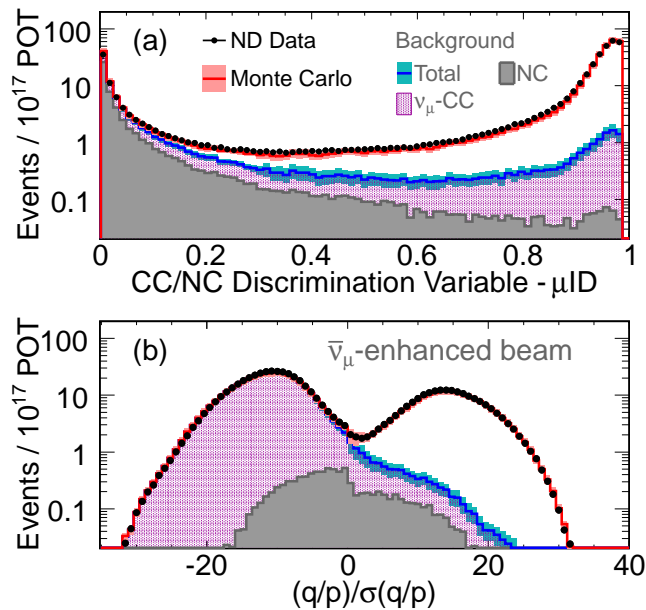


FIG. 1: Event selection variables from the ND: (a) The variable, μID , used to select $\bar{\nu}_\mu/\bar{\nu}_\mu\text{-CC}$ events and reject NC events. (b) The reconstructed track charge/momentum q/p divided by the uncertainty $\sigma(q/p)$ reported by the track reconstruction algorithm. In both figures, we have applied all selection criteria except the one on the quantity being shown. Shaded bands show systematic uncertainties. The background histograms are stacked on top of each other.

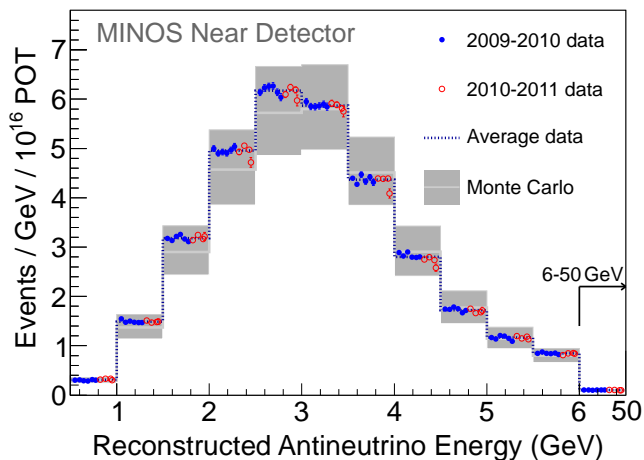


FIG. 2: The $\bar{\nu}_\mu\text{-CC}$ energy spectrum measured by the ND. The selection procedure described in the text has been applied. Each point represents one month of data. The shaded Monte Carlo band shows the combined effect of systematic uncertainties due to cross-sections, flux, energy scale and other sources.

ing $\frac{q/p}{\sigma(q/p)} > 0$ with a MC estimated efficiency/purity of 98.4%/94.7% in the ND and 98.8%/95.1% in the FD. The $\bar{\nu}_\mu$ background accepted by the selection is predominantly due to high energy muons with small curvature.

We reconstruct the neutrino energy by summing muon and hadronic shower energies. The muon energy is measured using track range and curvature. We reconstruct the hadronic shower energy using three variables: the sum of the reconstructed energy deposited by showers that start within 1m of the track vertex; the sum of the energy in the two largest showers reconstructed in the event; and the length of the longest shower. We use these three variables in a second kNN algorithm and estimate the shower energy as the mean true hadronic energy of the $k = 400$ closest MC events. This technique improves the hadronic energy resolution when compared to a method which uses only the energy deposited by the largest shower, increases the statistical sensitivity to $\Delta\bar{m}^2$ by 10%, and was previously used to analyze $\bar{\nu}_\mu$ disappearance [4, 23].

Data from the ND are used to predict the neutrino energy distribution at the FD. Though both detectors have the same segmentation and very similar average magnetic fields, for economic reasons the ND is smaller and asymmetric about the magnetic field coil and is more coarsely instrumented with scintillator in the downstream “muon spectrometer” region [19]. In addition, the ND coil occupies a larger fractional area than the FD coil and more muons enter it. In the ND data, we observe a reconstruction failure rate of 6.1%, mostly associated with tracks entering the coil region, but the MC predicts 4.2%. Previously, we dealt with this issue by assigning a systematic error. Now, we remove ND events with a track that ends less than 60cm from the coil. We also remove events with a track that ends on the side of the coil opposite the beam centroid. The new event selection decreases the efficiency to 53% in the ND, but reduces the data/MC failure rates to 1.4%/0.9%. The selected sample contains the same classes of neutrino scattering processes as are present at the FD, and our results are not significantly more vulnerable to cross-section uncertainties. We applied the new selection and shower energy reconstruction to the 2009-2010 data and found that the best fit parameters shifted by only $\delta(\Delta\bar{m}^2) = +1.0 \times 10^{-4} \text{ eV}^2$ and $\delta(\sin^2(2\theta)) = -3.6 \times 10^{-2}$.

A total of 2.98×10^{20} protons were delivered to the graphite target during the data-taking periods. We impose a series of data and beam quality [3, 24, 25] requirements which reduce the analyzable exposure to 2.95×10^{20} POT (99.0% livetime) at the FD, and 2.73×10^{20} POT (91.8% livetime) at the ND. The uncertainty in the livetime is negligible, and the high and largely overlapping livetime in both detectors assures that our results are not sensitive to beam effects that would cause the number of events per POT to vary.

Under normal conditions, the ND measures about 2400

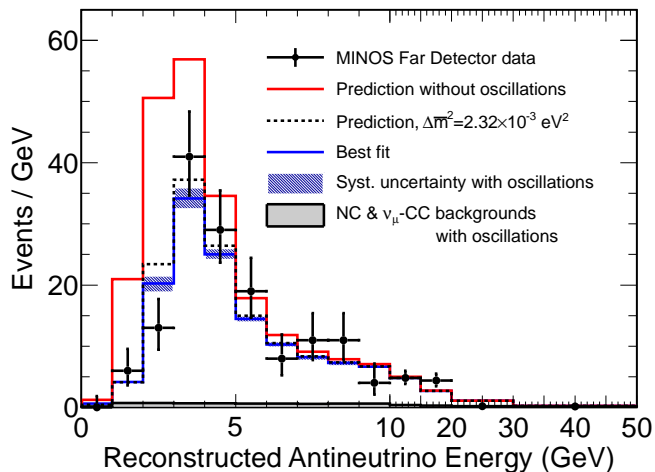


FIG. 3: The reconstructed energy of FD $\bar{\nu}_\mu$ -CC events. These data are fit to produce the 2009-2011 contour shown in Fig. 4. The band displays the effect of systematic uncertainties.

$\bar{\nu}_\mu$ -CC events per day in the oscillation energy region ($E_\nu < 6$ GeV). These data are essential for monitoring the neutrino beam and the quality of the experiment. Figure 2 shows the reconstructed $\bar{\nu}_\mu$ energy distribution measured in each month during the data-taking periods. With the exception of Feb. 2011 (the last point in each bin in Fig. 2), all months are in statistical agreement, and we expect a constant counting rate per POT at the FD. Part of the February dataset was taken after the neutrino target's cooling system had failed, leaking water into the target canister. This resulted in a decrease in the neutrino flux of 4% from 0-6 GeV when integrated over the entire month. The decrease is adequately modeled by our beam simulation, and we account for it at the FD using the ND data.

Measurements of the beam position and width at the target, the position of the remnant proton beam at the end of the decay pipe, and the integrated muon flux from meson decays in the pipe, all further indicate that the expected number of $\bar{\nu}_\mu$ -CC per POT is constant at the FD. Using the proton beam and monitors we measured the target and horn misalignments as well as the residual magnetic field in the neck of the focusing horns [26]. We conclude that these effects introduce $\ll 1\%$ uncertainty in the rate at the FD.

Events at the FD are read out in a $100\ \mu\text{s}$ window surrounding the $10\ \mu\text{s}$ long beam spill [27]. We select events coincident with the beam spill that have a vertex in the fiducial volume and a track identified as a muon by μID . We remove cosmic-ray background by requiring that the cosine of the angle between the track and beam direction be > 0.6 . A total of 521 events satisfy our criteria, 273 in the 2009-2010 dataset and 248 in 2010-2011. Using the muon charge, we identify 328 as ν_μ and 193 as $\bar{\nu}_\mu$. We apply the selection to 37.7×10^7

readout windows taken in anticoincidence with the beam during 2005-2011 and estimate a cosmic-ray background of 0.8 events. We monitor detector and reconstruction performance by measuring the rate of cosmic-ray muons traversing the detector before and after the beam spill. The rates in each data-taking period, 0.38 ± 0.03 Hz in 2009-2010 and 0.41 ± 0.04 Hz in 2010-2011, are consistent.

We predict the $\bar{\nu}_\mu$ energy spectrum at the FD by first correcting the ND spectrum for inefficiency and backgrounds. We then transfer that spectrum to the FD using a two dimensional "beam matrix" [3]. We predict 273 events if $\bar{\nu}_\mu$ do not oscillate, including 3.5 NC and 10.8 ν_μ -CC [31]. The energy spectra are shown in Fig. 3. Oscillations are incorporated into the prediction according to Eq. 1. Maximizing the binned log-likelihood yields

$$\begin{aligned} \Delta\bar{m}^2 &= [2.62^{+0.31}_{-0.28}(\text{stat.}) \pm 0.09(\text{syst.})] \times 10^{-3} \text{eV}^2 \\ \sin^2(2\bar{\theta}) &= 0.95^{+0.10}_{-0.11}(\text{stat.}) \pm 0.01(\text{syst.}) \\ \sin^2(2\bar{\theta}) &> 0.75 \quad (90\% \text{ C.L.}) \end{aligned}$$

with $p = 35.3\%$ at best fit [32]. When analyzing the 2010-11 alone we obtain $\Delta\bar{m}^2 = [2.26^{+0.27}_{-0.29}(\text{stat.}) \pm 0.09(\text{syst.})] \times 10^{-3} \text{eV}^2$, $\sin^2(2\bar{\theta}) > 0.79$ (90% C.L.) with $p = 14.5\%$.

The systematic errors stated above were evaluated by computing the standard deviation in the best fit parameters as the fits were repeated using MC samples that were shifted in accordance with uncertainties in neutrino cross-sections; the beam matrix and relative FD normalization; NC and ν_μ -CC backgrounds; the relative FD to ND energy calibration; the absolute muon energy scale; and the absolute hadronic energy scale, including final state hadronic interactions. The input uncertainties are as in our previous analyses [1, 4] and were derived from in-situ data, bench tests of detector and beam components, a test beam experiment, and published neutrino and hadron cross-sections [3, 28]. We increased the uncertainty in the axial-vector mass from 15% to 30% to account for additional uncertainties in $\bar{\nu}_\mu$ quasi-elastic scattering [29].

w

The confidence regions shown in Fig. 4 were calculated according to the unified procedure of [30] and incorporate both statistical and systematic uncertainties. We assess the consistency of the ν_μ and $\bar{\nu}_\mu$ measurements by doing a joint ($\Delta\bar{m}^2 = \Delta m^2, \sin^2(2\bar{\theta}) = \sin^2(2\theta)$) fit to the data to establish the null hypothesis. We then perform four-parameter ($\Delta\bar{m}^2, \Delta m^2, \sin^2(2\bar{\theta}), \sin^2(2\theta)$) fits on an ensemble of ν_μ and $\bar{\nu}_\mu$ MC experiments generated at the joint best fit. The joint fit had a larger likelihood than $p = 42\%$ of the four parameter fits, indicating consistency between ν_μ and $\bar{\nu}_\mu$.

In conclusion, we have used a $\bar{\nu}_\mu$ -enhanced Fermilab accelerator beam and detectors that discriminate ν_μ from $\bar{\nu}_\mu$ to make the most precise measurement of $\Delta\bar{m}^2$. Our results remove the tension reported in [1] and establish

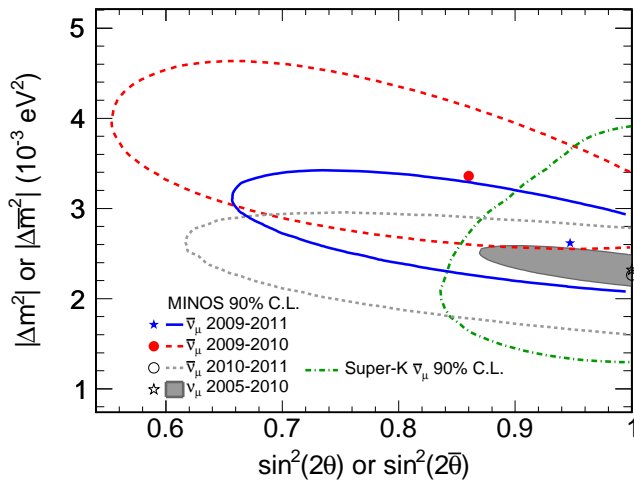


FIG. 4: Confidence regions calculated by fitting the FD data with an energy spectrum predicted from the ND but modified to incorporate oscillations via Eq. 1. The regions include statistical and systematic uncertainties. The $\bar{\nu}_\mu$ 2009-2011 contour is derived from the energy spectrum shown in Fig. 3.

consistency between ν_μ and $\bar{\nu}_\mu$ oscillations at $L/E \approx 200$ km/GeV.

This work was supported by the U.S. DOE; the United Kingdom STFC; the U.S. NSF; the State and University of Minnesota; the University of Athens, Greece; Brazil's FAPESP, CNPq and CAPES; and the Jeffress Memorial Trust. We are grateful to the Minnesota Department of Natural Resources and the personnel of the Soudan Laboratory and Fermilab.

* Deceased.

[1] P. Adamson et al. (MINOS), Phys. Rev. Lett. **107**, 021801 (2011).
 [2] D. G. Michael et al. (MINOS), Phys. Rev. Lett. **97**, 191801 (2006).
 [3] P. Adamson et al. (MINOS), Phys. Rev. D **77**, 072002 (2008).
 [4] P. Adamson et al. (MINOS), Phys. Rev. Lett. **106**, 181801 (2011).
 [5] Y. Ashie et al. (Super-Kamiokande), Phys. Rev. Lett. **93**, 101801 (2004).
 [6] W. W. M. Allison et al. (Soudan-2), Phys. Rev. D **72**, 052005 (2005).
 [7] M. Ambrosio et al. (MACRO), Eur. Phys. J. C. **36**, 323 (2004).
 [8] M. H. Ahn et al. (K2K), Phys. Rev. D **74**, 072003 (2006).

[9] Q. R. Ahmad et al. (SNO), Phys. Rev. Lett. **89**, 011301 (2002).
 [10] S. Abe et al. (KamLAND), Phys. Rev. Lett. **100**, 221803 (2008).
 [11] Z. Maki, M. Nakagawa, and S. Sakata, Prog Theor. Phys. **28**, 870 (1962); B. Pontecorvo, Zh. Eksp. Teor. Fiz. **53**, 1717 (1967) [Sov. Phys. JETP **26**, 984 (1968)]; V. N. Gribov and B. Pontecorvo, Phys. Lett. B **28**, 493 (1968).
 [12] R. N. Mohapatra and G. Senjanovic, Phys. Rev. Lett. **44**, 912 (1980).
 [13] M. Fukugita and T. Yanagida, Phys. Lett. B **174**, 45 (1986).
 [14] K. Nakamura et al. (Particle Data Group), J. Phys. G **37**, 075021 (2010).
 [15] S. J. Parke, in *Neutrino oscillations: Present status and future plans*, edited by J. A. Thomas and P. L. Vahle (World Scientific, 2008), also published as FERMILAB-PUB-07-767-T.
 [16] T. Araki et al. (KamLAND), Phys. Rev. Lett. **94**, 081801 (2005).
 [17] In matter $P(\nu_\mu \rightarrow \nu_\mu)$ and $P(\bar{\nu}_\mu \rightarrow \bar{\nu}_\mu)$ can differ by as much as 0.1% due to $\nu_\mu \leftrightarrow \nu_e$ mixing and ν_e and $\bar{\nu}_e$ scattering on electrons. This effect is too small to be observed in our experiment.
 [18] L. Wolfenstein, Phys. Rev. D **17**, 2369 (1978).
 [19] D. G. Michael et al. (MINOS), Nucl. Instrum. Meth. A **596**, 190 (2008).
 [20] Accounting for flux and cross-sections, the $\nu_\mu(\bar{\nu}_\mu)$ enhanced beam consists of 91.7%(58.1%) ν_μ , 7.0%(39.9%) $\bar{\nu}_\mu$ and 1.3%(2.0%) $\nu_e + \bar{\nu}_e$.
 [21] K. Abe et al. (T2K) (2012), arXiv:hep-ex/1201.1386.
 [22] R. Ospanov, Ph.D. Thesis, University of Texas at Austin (2008).
 [23] C. Backhouse, D.Phil. Thesis, Oxford University (2011).
 [24] S. Kopp, arXiv:physics/0508001.
 [25] K. Anderson et al., Tech. Rep., Fermilab (1998), FERMILAB-DESIGN-1998-01.
 [26] A zero field is expected due to symmetry around the beam axis. We measure a 1×10^{-2} mrad deflection of the primary proton beam, corresponding to $B \cdot dl = 43$ Gm.
 [27] The window is defined by GPS time-stamping each beam extraction and transmitting the time stamp over the internet to the FD, which buffers data to cope with latency.
 [28] S. Dytman, H. Gallagher, and M. Kordosky (2008), arXiv:hep-ex/0806.2119.
 [29] A. Bodek, H. S. Budd and M. E. Christy, Eur. Phys. J. C **71**, 1726 (2011).
 [30] G. J. Feldman and R. D. Cousins, Phys. Rev. D **57**, 3873 (1998).
 [31] ν_μ are assumed to oscillate with $\Delta m^2 = 2.32 \times 10^{-3} eV^2$ and $\sin^2(2\theta) = 1$.
 [32] The “p-value”, p , is the probability, assuming our fit hypothesis is true, of obtaining data more incompatible with our hypothesis than the data we actually observe. See the discussion in section 33.2.2 of [14].

This figure "rhc_contours_olldrhc_cc_r7_FC_prlColor_superk_center_v2.png" is available

<http://arxiv.org/ps/1202.2772v1>

This figure "RecoE_finalprl_thin_v3.png" is available in "png" format from:

<http://arxiv.org/ps/1202.2772v1>

This figure "predictions_AllRuns_data_best_cc_prIColor_no_exposure_v3.png" is av

<http://arxiv.org/ps/1202.2772v1>

This figure "qp_stacked.png" is available in "png" format from:

<http://arxiv.org/ps/1202.2772v1>

This figure "roid_stacked.png" is available in "png" format from:

<http://arxiv.org/ps/1202.2772v1>